THE JOURNAL OF PHYSICAL CHEMISTRY B
A JOURNAL OF THE AMERICAN CHEMICAL SOCIETY

pubs.acs.org/JPCB

Article

Modeling Liquid Water by Climbing up Jacob's Ladder in Density Functional Theory Facilitated by Using Deep Neural Network Potentials

Published as part of The Journal of Physical Chemistry virtual special issue "125 Years of The Journal of Physical Chemistry".

Chunyi Zhang, Fujie Tang, Mohan Chen, Jianhang Xu, Linfeng Zhang, Diana Y. Qiu, John P. Perdew, Michael L. Klein,* and Xifan Wu*

Cite This: https://doi.org/10.1021/acs.jpcb.1c03884

Read Online

ACCESS | Metrics & More | Article Recommendations

ABSTRACT: Within the framework of Kohn–Sham density functional theory (DFT), the ability to provide good predictions of water properties by employing a strongly constrained and appropriately normed (SCAN) functional has been extensively demonstrated in recent years. Here, we further advance the modeling of water by building a more accurate model on the fourth rung of Jacob's ladder with the hybrid functional, SCAN0. In particular, we carry out both classical and Feynman path-integral molecular dynamics calculations of water with the SCAN0 functional and the isobaric–isothermal ensemble. To generate the equilibrated structure of water, a deep neural network potential is trained from the atomic potential energy surface based on *ab initio* data obtained from SCAN0 DFT calculations. For the electronic properties of water, a separate deep neural network potential is trained by using the Deep Wannier method based on the maximally localized Wannier functions of the equilibrated trajectory at the SCAN0 level. The structural, dynamic, and electric properties of water were analyzed. The hydrogen-bond structures, density, infrared spectra, diffusion coefficients, and dielectric constants of water, in the electronic ground state, are computed by using a large simulation box and long simulation time. For the properties involving electronic excitations, we apply the GW approximation within many-body perturbation theory to calculate the quasiparticle density of states and bandgap of water. Compared to the SCAN functional, mixing exact exchange mitigates the self-interaction error in the meta-generalized-gradient approximation and further softens liquid water toward the experimental direction. For most of the water properties, the SCAN0 functional shows a systematic improvement over the SCAN functional. However, some important discrepancies remain. The H-bond network predicted by the SCAN0 functional is still slightly overstructured compared to the experimental results.

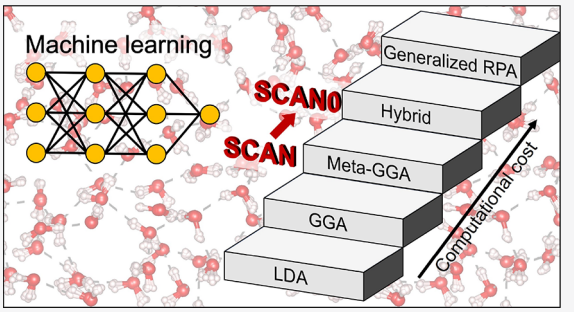

INTRODUCTION

Water is arguably the most important substance on this planet. The remarkable functionalities of liquid water arise from a series of its unique and mysterious properties. The density anomaly enables water to freeze from the top down, which is essential to sustain the life and natural evolution on earth;[1,2] the frequent autoionization processes and the subsequent fast proton transport determine its amphoteric nature that underpins all the acid–base chemical reactions;[3,4] the hydrophobic effect in an aqueous environment is believed to be the driving force behind protein folding.[5,6] To unravel all these biological and chemical processes, a genuinely predictive model of water holds the key. Not surprisingly, understanding the hydrogen (H)-bond structure of water continues to command intense attention from both experimentalists and theoreticians.[4,7−18]

Advanced experimental techniques have been extensively applied to the study of water. The arrangement of water molecules can be probed by neutron scattering or X-ray diffraction experiments;[9,10] the H-bond dynamics are detectable by infrared (IR),[19,20] sum-frequency vibrational,[21−23] and pump–probe[24] spectroscopy measurements; the photoemission[8] and X-ray absorption[7] spectra provide the electronic structure information about water. Nevertheless, the available

Received: May 3, 2021

experimental techniques only provide ensemble-averaged information about water. For insight into the microscopic details, scientists in the field mainly rely on the theoretical modeling of molecules to further understand the structure, dynamics, and electronic properties of water. To rationalize the experimental data, an accurate first-principles theory is crucial because its predictions are based on quantum mechanical principles without any empirical input. In this regard, *ab initio* molecular dynamics (AIMD)[25] provides an ideal framework to model liquid water at the microscopic level. In AIMD, the driving force at each time step is determined by density functional theory (DFT).[26,27]

In DFT, the interacting many-electron problem in any condensed system can be exactly mapped onto a single-body problem with the inclusion of an exchange-correlation (XC) term. However, the predictive power of DFT crucially depends on the practical form of the XC functional approximation. The accuracy can be systematically improved by climbing up Perdew's metaphorical Jacob's ladder[28] of XC functionals, with each rung considering additional delicate physical effects. Climbing up Jacob's ladder, which consists of five rungs, to study water is a nontrivial task as more accurate XC functionals require significantly more computational resources. Water is a collection of molecules that are loosely bonded by positively charged H atoms pointing toward negatively charged oxygen (O) atoms, thereby forming the H-bonds that govern many peculiar properties of water. Because of the delicate nature of the H-bond network, it has been widely accepted that the accurate prediction of water properties demands higher rungs of Jacob's ladder than ordinary materials.[13] The first rung of Jacob's ladder is the local density approximation (LDA),[29,30] which is parametrized based on the uniform electron gas and tends to minimize the inhomogeneity of electron density. While the overestimation of chemical bonds by LDA was observed as a general trend,[31,32] the significantly overestimated H-bond strength means that LDA fails in even qualitatively predicting water properties. Also, first-principles MD calculations of water by LDA only lasted for a short time period in the 1990s. In the following 20 years, simulations of water were dominated by utilizing the second rung of XC functionals with the generalized gradient approximation (GGA).[33,34] By introduction of the electron density gradient, the GGA functional allows more constraints to be satisfied than LDA. In particular, the nonempirical GGA functional by Perdew, Burke, and Ernzerhof (PBE)[35] satisfies both the constraints on the electron-correlation hole and electron-correlation energy. PBE-GGA weakens the H-bond strengths toward the experimental direction.[13] Revisions of PBE such as revPBE[36] are constructed by satisfying fewer physical constraints than PBE. However, GGA also has limitations. PBE-GGA intrinsically lacks the intermediate- and long-range van der Waals (vdW) interactions and largely underestimates the liquid water density, notably, incorrectly yielding denser ice than water.[37] Adding explicit dispersion corrections, such as Grimme (D3)[38,39] and Tkatchenko−Scheffler (TS)[40] vdW corrections, to the GGA functional can significantly soften the structure of water and improve the density toward the experimental direction.[11,13,41] Recently, the nonempirical meta-GGA strongly constrained and appropriately normed (SCAN) functional[42,43] was proposed as a general-purpose *ab initio* functional that belongs to the third rung of Jacob's ladder. With the introduction of kinetic energy density together with a dimensionless variable, SCAN satisfies 17 known constraints on XC functionals as well as the tight lower bound on the exchange energy which has been elusive in PBE-GGA on the second rung of Jacob's ladder. SCAN was found to provide a substantially more accurate description of water as compared to GGAs, including structural, electronic, and dynamical properties.[14,44,45] Most importantly, SCAN includes intermediate-range vdW interactions inherently, and the resulting density of water is 1.050 g/cm^3, which is much closer to the experimental value of 0.997 g/cm^3, as compared to the density of ∼0.850 g/cm^3 from PBE-GGA functionals.[14] Besides the accurate prediction of the density difference between water and hexagonal ice at ambient conditions,[14] the recent combination of the SCAN functional with a machine learning potential found that the SCAN functional can also correctly predict the relative stability between hexagonal ice and cubic ice.[46] In the past few years, SCAN has been one of the most commonly used nonempirical XC functionals in the studies of water.

Notwithstanding the above significant progress, challenges remain. Both GGA and meta-GGA functionals suffer from the self-interaction error.[47,48] The spurious interaction of the electron with itself leads to excessive proton delocalization and an artificially strengthened H-bond.[49] The overestimated H-bond strength is evidenced by the red-shift of the IR stretching band predicted by SCAN in comparison with experiment.[50] The above is also consistent with the slightly overstructured oxygen−oxygen pair distribution predicted by SCAN as compared to the neutron scattering data.[14] Recently, Lambros et al. assessed the accuracy of the SCAN functional by investigating the effects of the exact exchange using the MB-pol approach and found that adding different fractions of exact exchange to the SCAN functional leads to substantial changes in the structure of liquid water.[51] Furthermore, most AIMD simulations of water so far have assumed classical nuclei. However, the light hydrogen atom deviates from classical behavior significantly, even at room temperature.[52−54] The Feynman discretized path-integral (PI) method combined with AIMD can treat the nuclear quantum effect (NQEs).[55,56] But for reasons of computational cost, the PI-AIMD simulations have not yet been widely applied to water. More disturbingly, many thermodynamic properties of water are difficult to predict by DFT based on currently available computational resources. Standard AIMD simulations are typically performed for a time scale of tens of picoseconds, and the system size is limited to a simulation box containing a few tens to a hundred or so water molecules. In water, the time for the H-bond to break and re-form is typically at the picosecond scale.[57] Therefore, the H-bond structure in water can be faithfully predicted within tens of picoseconds by AIMD simulation. However, for many macroscopic properties, such as diffusivity and dielectric constant, the converged predictions require much longer simulation time and larger system size. To approach the thermodynamic limit, at least thousands of water molecules are necessary to be considered in the simulation box, which is simply impossible for AIMD.

To address the above issues, we ascend Jacob's ladder of DFT to the fourth rung using the SCAN0 hybrid functional to study liquid water with NQEs considered simultaneously by the PI method. The predictions of converged thermodynamic properties are largely facilitated by employing state-of-the-art deep potential molecular dynamics (DPMD).[58−60] The many-body potential and interatomic forces needed for DPMD are obtained from a deep neural network that is trained with

https://doi.org/10.1021/acs.jpcb.1c03884
J. Phys. Chem. B XXXX, XXX, XXX−XXX

SCAN0 DFT data. DPMD has recently been demonstrated to be able to accurately model the structure of pure water with an accuracy at the DFT level and with the low computational cost of a classical force field.[58,61] For the electronic properties, we adopt the Deep Wannier[62] neural network model, which is trained with the positions of centers of the maximally localized Wannier functions[63,64] that are obtained from SCAN0 DFT calculations. We focus on the SCAN0 results at 330 K so these results can be compared directly with previous simulations of water with the SCAN functional,[14,50] which were also performed at this temperature. These results reveal the physical corrections caused by including exact exchange and nuclear quantum effects. At the same time, results for SCAN0 at 300 K are also presented for a direct comparison with 298/300 K experimental results. Compared to the third rung of Jacob's ladder of SCAN, SCAN0 presents a better description of liquid water in terms of structure, dynamics, and electronic properties. By mixing 10% exact change as suggested for an earlier meta-GGA functional,[65] SCAN0 mitigates the self-interaction error. The less polarizable water together with the NQEs on the protons yields a liquid structure softened toward the experimental direction compared with SCAN. The predicted dynamic properties such as IR spectra and diffusivities and the electric properties such as dielectric constants are in good agreement with available experiments. Finally, we compute the quasiparticle band structure of liquid water based on Hedin's GW approximation[66] as implemented in the BerkeleyGW package.[67,68] The predicted density of states (DOS) and bandgap are in reasonable agreement with recent photoemission spectroscopy (PES) experiments.

METHODS

Training Process of the SCAN0 Deep Potential Model. To construct an accurate and transferable SCAN0 path-integral deep potential model with a minimal number of the expensive SCAN0 DFT data, an active machine learning procedure called deep potential generator (DP-GEN)[59] was adopted. The procedure is summarized as follows:

(1) Considering that the molecular configurations predicted by SCAN and SCAN0 are close to each other, 900 configurations were uniformly extracted from the 64-molecule 11 ps SCAN PI-AIMD trajectory reported in ref 69. The total potential energy E and ionic forces $\mathbf{F}_i$ of each atom i of these configurations were calculated by using Quantum ESPRESSO (QE)[70] with the SCAN0 XC functional. The Hamann–Schlüter–Chiang–Vanderbilt (HSCV) pseudopotentials[71,72] with an energy cutoff of 150 Ry were employed. The obtained E and $\mathbf{F}_i$ together with atomic positions were adopted as the initial training data.

(2) The DeePMD-kit package[73] was used to train four deep potential models independently for 10^6 steps. The differences between the training processes of the four deep potential models were the initialization random parameters and the activation function. Two models were trained by using the Tanh activation function, while the other two models were trained by using the GELU activation function. The training followed the procedure described in refs 58 and 60. First, the input data were transformed to local coordinate frames for every atom and its neighbors inside a cutoff distance of 6 Å to preserve the translational, rotational, and permutational symmetries. Afterward, the deep neural network parameters were optimized by the Adam method[74] with the loss function

$$\mathcal{L}(p_\epsilon, p_f) = p_\epsilon \Delta\epsilon^2 + \frac{p_f}{3n}\sum_i |\Delta\mathbf{F}_i|^2$$

where $\Delta\epsilon$ and $\Delta\mathbf{F}_i$ represent the differences between the training data and current deep potential prediction for the quantities $\epsilon \equiv E/n$ and $\mathbf{F}_i$, respectively, n is the number of atoms, and p_ϵ and p_f are tunable prefactors. In the training process, p_ϵ progressively increases from 0.02 to 1, while p_f progressively decreases from 1000 to 1.

(3) To explore the potential energy surface, ten independent PI-DPMD simulations were performed in the NpT ensemble at 1 bar and 330/300 K for 100 ps with a time step of 0.5 fs by using the i-PI code[56] in conjunction with the DeePMD-kit package.[73] A periodically replicated cubic cell containing 64 water molecules was used. The nuclear degrees of freedom were sampled by using eight beads with a colored-noise generalized Langevin equation thermostat[75,76] to accelerate the convergence of the quantum distribution. The pressure was controlled by using an isotropic barostat as implemented in the i-PI code with a time constant associated with the dynamics of the piston of 200 fs. The cell was thermostated by another generalized Langevin equation thermostat[77,78] to enhance sampling efficiency. For each PI-DPMD simulation, all of the four deep potential models were used to predict the force acting on each atom at each time step, but only one model randomly selected from the four models was used to propagate the trajectory.

(4) The convergence of the PI-DPMD simulations was checked. Following ref 59, the maximum standard deviation of the predicted atomic forces $\zeta = \max_i\sqrt{\langle \| \mathbf{f}_i - \overline{\mathbf{f}}_i \|^2 \rangle}$ was adopted as an indicator for the convergence, where $\overline{\mathbf{f}}_i = \langle \mathbf{f}_i \rangle$ is the average force on atom i predicted by the four different deep potential models. If the input training data set can cover the potential energy surface, the four forces predicted by the four models at each PI-DPMD step will agree with each other, and ζ will be close to zero. In this work, when the configurations that have $\zeta > 0.2$ eV/Å account for <0.005% of all the PI-DPMD configurations, the models were considered to be converged. Otherwise, 50–400 configurations that have $\zeta > 0.2$ eV/Å were extracted. The force and energy of these configurations were calculated by using QE with the SCNA0 using the same DFT parameters as step one. The new DFT results were added to the training data set, and the loop was repeated until obtaining a converged deep potential model.

One converged deep potential model was employed to conduct the production run, which was trained by using 7349 SCAN0 DFT configurations. Note that the number of training configurations adopted here is not the minimum number of configurations needed for convergence because, in the first few iterations, configurations that have $\zeta > 0.05$ eV/Å were also added to the training data set. These "extra" configurations are not essential for the convergence and will not affect the simulation results. To verify the reliability of the deep potential model, we also conducted a SCAN0 AIMD simulation of liquid water in the NpT ensemble at 1 bar and 330 K for 20 ps with a 64-molecule cell using QE. HSCV pseudopotentials[71,72] with an energy cutoff of 130 Ry were adopted. As shown in Figure 1, the RDFs predicted by AIMD and DPMD simulations agree well with each other, which proved the convergence of the SCAN0 deep potential model.

To predict the electronic properties, the Deep Wannier[62] method was applied to build another deep potential model to

https://doi.org/10.1021/acs.jpcb.1c03884
J. Phys. Chem. B XXXX, XXX, XXX–XXX

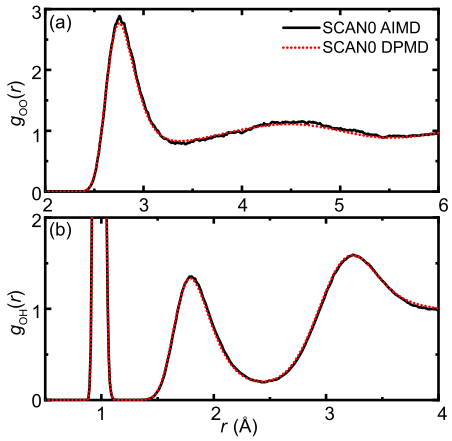

Figure 1. (a) $g_{OO}(r)$ and (b) $g_{OH}(r)$ of liquid H_2O from SCAN0 AIMD and DPMD simulations at 1 bar and 330 K.

map input atomic coordinates into output Wannier centers. First, the Wannier centers of the 7349 SCAN0 DFT configurations were calculated by using QE. Each water molecule i has four valence Wannier centers. The centroid of the four Wannier centers $\mathbf{r}_w^i = \frac{1}{4}\sum_{c=1}^{4}\mathbf{r}_{w_c}^i$ and the atomic positions were adopted as the input training data and trained for 10^6 steps by using the DeePMD-kit package.[73]

Classical and Quantum DPMD Simulations. The SCAN0 deep potential model was applied to conduct both DPMD and PI-DPMD simulations at 1 bar and 330/300 K with a simulation cell containing 512 water molecules. Specially, the dielectric constant and diffusion coefficient were calculated by using cells containing 64−4096 molecules. All static properties were calculated by using the *NpT* ensemble. To avoid the influence of the thermostat and barostat on the dynamics, all dynamical properties were calculated by using the microcanonical (*NVE*) ensemble with the cell size fixed at the value obtained from the *NpT* simulation. The DPMD simulation was performed by using LAMMPS[79] in conjunction with the DeePMD-kit package[73] for 2 ns with the first 100 ps discarded for equilibrium. The PI-DPMD simulation was conducted by using the i-PI code[56] in connection with the DeePMD-kit package[73] for 500 ps with the first 100 ps discarded for equilibrium. The PI-DPMD simulation parameters related to nuclear and cell dynamics were the same as those adopted in step three of the deep potential training process.

Calculation of the Electronic DOS and Bandgap. The electronic DOS and bandgap of liquid water were calculated at the level of DFT and G_0W_0. All the DFT calculations reported in this work are performed at the level of SCAN0. A 0.1 eV Gaussian broadening factor was adopted for the computed eigenstates. The SCAN0 classical DFT result was calculated based on 200 snapshots that uniformly extracted from the 2 ns

Table 1. Structural, Dynamical, and Electronic Properties of Liquid Water Predicted by SCAN0 DPMD and PI-DPMD Simulations at 330 and 300 K in Comparison with the SCAN Results at 330 K and the Experimental Results at 298 and 300 K (298 K for Refs 9, 19, 20, and 80−83; 300 K for Refs 84−86)[a]

property	method	T (K)	d_{OH} (Å)	N_{HB}	ρ (g/cm^3)
structural (H_2O)	exp	298/300	1.01[9]		0.997[84]
	SCAN AIMD	330	0.984[14]	3.61[14]	1.050[14]
	SCAN0 DPMD	330	0.980	3.58	1.030
	SCAN0 PI-DPMD	330	0.999	3.49	1.041
	SCAN0 DPMD	300	0.981	3.71	1.032
	SCAN0 PI-DPMD	300	1.000	3.61	1.046

property	method	T (K)	ν_T (cm^{-1})	ν_L (cm^{-1})	ν_B (cm^{-1})	ν_S (cm^{-1})	D (Å^2/ps)	τ_2 (ps)
dynamical (D_2O)	exp	298/300	186[19]	486[19]	1209[19]	2498[19]	0.20[85]	2.4[86]
	SCAN AIMD	330	172[50]	483[50]	1207[50]	2448[50]		
	SCAN0 DPMD	330	227	486	1219	2507	0.26	1.9
	SCAN0 DPMD	300	213	514	1222	2479	0.12	4.6
dynamical (H_2O)	exp	298/300	176[20]	615[20]	1646[20]	3406[20]	0.24[85]	1.7−2.6[80,81]
	SCAN	330					0.26[87]	3.3[87]
	SCAN0 DPMD	330	208	675	1667	3475	0.29	1.7
	SCAN0 DPMD	300	207	729	1669	3408	0.13	4.1

property	method	T (K)	μ (D)	$\epsilon_{2a_1-1b_1}$ (eV)	$\epsilon_{1b_2-1b_1}$ (eV)	$\epsilon_{3a_1-1b_1}$ (eV)	bandgap (eV)	ϵ
electronic (H_2O)	exp	298/300	2.9 ± 0.6[82]	−19.7[88]	−6.2[88]	−2.3[88]	8.7 ± 0.5[89]	78.39[83]
	SCAN AIMD (DFT)	330	2.97[14]	−18.9[14]	−5.7[14]	−2.0[14]		
	SCAN0 DPMD (DFT)	330	2.96	−19.4	−5.8	−2.0	5.1	76.83
	SCAN0 PI-DPMD (DFT)	330	3.08	−19.4	−5.6	−2.0	4.6	84.34
	SCAN0 PI-DPMD (G_0W_0)	330		−19.4	−6.4	−2.6	7.5	
	SCAN0 DPMD (DFT)	300	3.01	−19.4	−5.8	−2.0	5.1	95.33
	SCAN0 PI-DPMD (DFT)	300	3.13	−19.4	−5.6	−2.0	4.6	97.57
	SCAN0 PI-DPMD (G_0W_0)	300		−19.4	−6.4	−2.6	7.5	

[a]The structural properties include the average O−H covalent bond length (d_{OH}), average number of H-bonds per water molecule (N_{HB}), and density (ρ). The dynamical properties include the peak positions of the four IR bands (ν_T, ν_L, ν_B, and ν_S), the diffusion coefficient (D), and the rotational correlation time (τ_2). The electronic properties include the dipole moment (μ), the binding energies of $2a_1$, $1b_2$, and $3a_1$ peaks with respect to the $1b_1$ peak in the electronic DOS, the bandgap, and the dielectric constant (ϵ). For the method column in the electronic part, the text outside/inside the parentheses represents the calculation method of the molecular/electronic structure.

https://doi.org/10.1021/acs.jpcb.1c03884
J. Phys. Chem. B XXXX, XXX, XXX−XXX

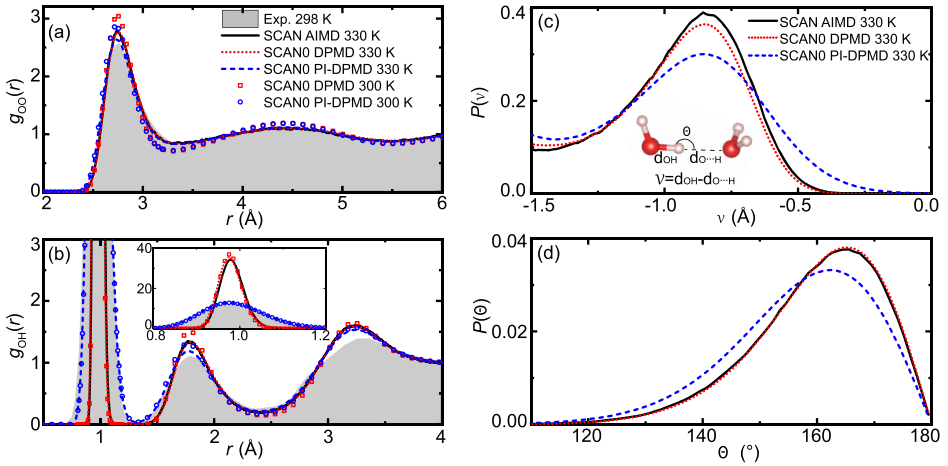

Figure 2. (a) $g_{OO}(r)$ and (b) $g_{OH}(r)$ of liquid H_2O from SCAN AIMD (330 K),[14] SCAN0 DPMD (330 and 300 K), and SCAN0 PI-DPMD (330 and 300 K) simulations as well as the diffraction experimental result (298 K)[9] reported in refs 9 and 90. The inset in (b) shows a rounded picture of the first peak of $g_{OH}(r)$. The corresponding probability distribution of (c) proton transfer coordinate, ν, and (d) OH···O angle, θ, of liquid H_2O at 330 K. The inset in (c) displays definitions of ν and θ.

64-molecule SCAN0 DPMD trajectory. The SCAN0 quantum DFT result was calculated based on 100 snapshots (each snapshot containing eight beads) that uniformly extracted from the 500 ps 64-molecule SCAN0 PI-DPMD trajectory, both SCAN0 classical and quantum DFT results containing 256 valence bands and 10 conduction bands.

The G_0W_0 calculation was performed by including dynamical dielectric screening effects using a generalized plasmon-pole model with the BerkeleyGW package.[67,68] Because of the large computational cost of the G_0W_0 method, the SCAN0 quantum result was calculated by using eight snapshots uniformly extracted from the 500 ps 32-molecule SCAN0 quantum trajectory, with the PBE functional as a starting point. For all the configurations, the dielectric function ϵ and the self-energy Σ were calculated by using 20000 bands to ensure convergence. The plane wave energy cutoff for ϵ was 30 Ry. A single gamma point was adopted. Overall, 128 occupied eigenstates and five empty eigenstates were calculated.

RESULTS AND DISCUSSION

In this section, the structural, dynamical, and electronic properties of liquid water predicted by the SCAN0 functional at 330 K are presented and compared with previous SCAN AIMD simulations at 330 K to demonstrate the physical corrections caused by adding exact exchange and nuclear quantum effects to results for the SCAN functional (see Table 1). To show a direct comparison with the 298/300 K experimental results, the SCAN0 results at 300 K are also presented in the table and the figures and are discussed in the last subsection.

Water Structure and Density Predicted at 330 K. We first inspect the structure of water predicted by various DFT functional approximations. To this end, we analyze the radial distribution functions (RDFs), which show the probability to find a given pair of atoms as a function of distance in real space. The resulting oxygen−oxygen and oxygen−hydrogen RDFs, $g_{OO}(r)$ and $g_{OH}(r)$, are shown in Figures 2a and 2b, respectively. The RDFs predicted by SCAN0 DPMD and SCAN0 PI-DPMD simulations are presented in the same figures with SCAN AIMD[14] and experimental results[9] for comparison.

Like all local and semilocal DFT functionals, the SCAN functional inherits the spurious self-interaction error, which yields an artificially strengthened tetrahedral structure and delocalized protons. By mixing a fraction (10%)[65] of exact exchange in SCAN0, the above self-interaction error is mitigated, which softens the liquid structure toward the experimental direction. The weakened H-bond strength by SCAN0 DPMD relative to SCAN AIMD is evidenced by the right shift of the first peak position of $g_{OO}(r)$ in Figure 2a, from 2.748 to 2.754 Å, and the second peak position of $g_{OH}(r)$ in Figure 2b, from 1.785 to 1.793 Å, both of which are closely associated with the H-bonds. The weaker H-bonds, in turn, enhance the covalency of water molecules in the liquid, as indicated by the shortened OH covalent bond length from 0.984 Å (SCAN AIMD) to 0.980 Å (SCAN0 DPMD). Not surprisingly, the weakened H-bonding also promotes the population of broken H-bonds. Adopting the definition of H-bonds by Chandler and Luzar,[16] the average calculated number of H-bonds per water molecule decreases from 3.61 (SCAN AIMD) to 3.58 (SCAN0 DPMD). The H-bond is highly directional. The forming or breaking of an H-bond critically depends on the geometric configurations as determined by the distance and angle between the H-bond donor and acceptor. As schematically shown in the inset of Figure 2c, the proton displacement along the stretching mode toward the H-bond acceptor facilitates the forming of H-bonds; on the other hand, the proton displacement along the libration mode tends to break H-bonds. The above two opposite effects are illustrated by the probability distributions of the proton transfer coordinate, ν, and OH···O angle, θ,[69,91] as shown in Figures 2c and 2d, respectively. It can be seen in Figure 2c that the broken H-bond by the SCAN0 functional originates from the reduced proton displacement along the H-bonding direction. In contrast, from SCAN to SCAN0 functional, the proton displacement along the libration direction barely changes as displayed in Figure 2d. This is consistent with the fact that the hybrid functional reduces the electronegativity of the lone pair electrons, which weakens the directional H-bonding strength. In accordance with the reduced directional H-bond strength, the water molecules are more loosely bonded with an increased O−O distance. Therefore, the predicted water density by SCAN0 DPMD is 1.030 g/cm^3, which is noticeably smaller

https://doi.org/10.1021/acs.jpcb.1c03884
J. Phys. Chem. B XXXX, XXX, XXX−XXX

than the density of 1.050 g/cm^3 predicted by SCAN AIMD simulation.[14]

In SCAN0 PI-DPMD simulations, the NQEs are incorporated in the modeling of water. The resulting $g_{OO}(r)$ and $g_{OH}(r)$ are presented in Figures 2a and 2b, respectively. In quantum simulations, the configuration space explored by protons is largely extended, in particular for the regions that are inaccessible to classical nuclei. Compared to classical simulations, PI-DPMD simulation results in a significantly broadened first peak of $g_{OH}(r)$, which is a typical effect reported in all path-integral simulations of water.[53,54,69,91−93] Besides the broadening effect, NQEs affect the H-bond network as well. Under the influence of NQEs, the protons are more delocalized along the direction of the stretching mode as well as the direction of the libration mode as shown in Figures 2c,d. The proton delocalization along the stretching mode yields more polarizable water with a larger electric dipole moment of 3.08 D compared to the classical water model of 2.96 D, which facilitates the formation of H-bonds. However, the proton delocalization along the libration mode tends to break more H-bonds. In SCAN0 PI-DPMD trajectories, the latter effect is more significant as evidenced by the largely shifted peak position away from H-bond direction (180°) in the OH···O angle distribution function in Figure 2d; in contrast, the center of the proton transfer probability function is less affected by NQEs. As a result of the above two competing NQEs, the average number of H-bonds per water molecule decreases from 3.58 to 3.49. At the same time, the water structure predicted by PI-DPMD is further softened toward the experimental direction as shown in Figures 2a,b, which is qualitatively similar to results predicted by the path-integral simulations that are based on PBE and BLYP GGA functionals.[91] Because of the more polarizable nature of water molecules under NQEs, the H-bonding force along the stretching mode becomes more attractive, which prefers a slightly more compactly packed water structure. Indeed, the predicted water density by SCAN0 PI-DPMD is 1.041 g/cm^3, which is slightly larger than 1.030 g/cm^3 as predicted by SCAN0 DPMD. The larger density under NQEs has also been widely reported in previous studies.[69,92,93]

Dynamic Properties Predicted at 330 K. The prediction of the quantum dynamic properties of water is still an open problem due to the application of the complex form of the real-time propagator in the current implementations of Feynman's path integral approach.[94] Therefore, the dynamical properties, including the IR spectra and the diffusivity presented in this work, are generated from classical simulations only.

IR Spectrum. IR spectroscopy is a powerful experimental technique to probe the vibrational properties of liquid water. The IR spectrum is sensitive to the underlying H-bond network in liquid water and is therefore widely adopted to study the microscopic structure of liquid water.[49,50,95] Within linear response theory, the IR absorption coefficient per unit length is given by the Fourier transform of the time correlation function of the overall dipole moment as follows:[96]

$$\alpha(\omega) = \frac{2\pi\beta\omega^2}{3cVn(\omega)} \int_{-\infty}^{+\infty} \mathrm{d}t\ \mathrm{e}^{-i\omega t} \left\langle \sum_{i,j} \boldsymbol{\mu}_i(0)\cdot\boldsymbol{\mu}_j(t) \right\rangle \quad (1)$$

where $n(\omega)$ is the refractive index, V is the volume, and $\beta = (k_B T)^{-1}$, with k_B and T being Boltzmann's constant and temperature, respectively. The dipole moment $\boldsymbol{\mu}_i$ of molecule i is calculated as $\boldsymbol{\mu}_i = 6\mathbf{r}^i_O + \mathbf{r}^i_{H_1} + \mathbf{r}^i_{H_2} - 2\sum_{c=1}^{4} \mathbf{r}^i_{w_c}$, where $\mathbf{r}^i_O$, $\mathbf{r}^i_{H_1}$, and $\mathbf{r}^i_{H_2}$ are the nuclear coordinates of the ith molecule and $\mathbf{r}^i_{w_c}$ $(c = 1-4)$ is the four Wannier centers assigned to the ith water molecule in the system, which is obtained from the Deep Wannier method in this work. Therefore, a precise prediction of the IR spectra demands an accurate description of both the molecular configuration and its dynamical electronic response.

We present the IR spectrum of heavy water predicted by SCAN0 DPMD simulation in Figure 3a. For comparison, the spectra computed from the SCAN AIMD simulation[50] and the experimental result[19] are also presented in the same figure. As shown in Figure 3a, the IR spectrum of liquid water displays four main spectral features that can be attributed to the hindered translation (ν_T), libration (ν_L), H−O−H bending (ν_B), and O−H stretching (ν_S) modes as a function of increasing frequency. The bending mode and stretching mode can be traced back to the molecular vibration of water vapor in the gas phase, while the hindered translation and libration modes arise from the collective motion of water molecules in the H-bond network. The IR spectra of D_2O in Figure 3a show that, compared to SCAN, SCAN0 improves all the four spectral features toward the experimental direction, in terms of both the spectral energies and their intensities. To elucidate the physical origin of the improved spectrum, we further decompose the IR spectrum into its intra- and intermolecular contributions.[95] The above can be rigorously implemented by separating the time-correlation function in eq 1 into

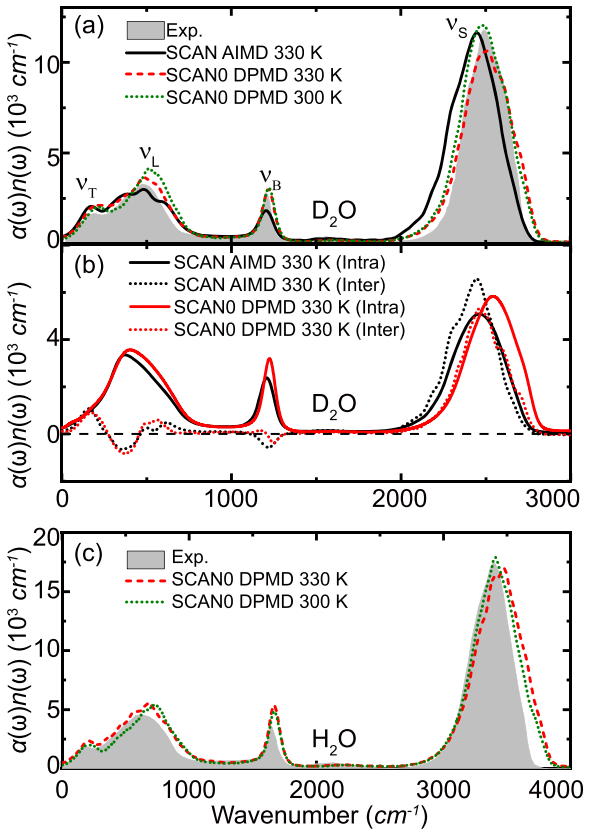

Figure 3. IR spectra of liquid D_2O predicted by SCAN AIMD (330 K),[50] SCAN0 DPMD (330 and 300 K), and the experiment (298 K).[19] (b) Decomposition of the IR spectra at 330 K in (a) into intra- and intermolecular contributions. (c) IR spectra of H_2O from SCAN0 DPMD simulations (330 and 300 K) and the experiment (298 K).[20]

https://doi.org/10.1021/acs.jpcb.1c03884
J. Phys. Chem. B XXXX, XXX, XXX−XXX

contributions from $i = j$ and $i \neq j$ terms utilizing the additive nature of the two-body correlation function. The resulting decompositions are shown in Figure 3b.

We first inspect the stretching band centered around 2500 cm^{-1}. According to previous studies, it was found that SCAN functional improves the underestimated stretching frequency compared to the PBE functional.[50] However, the predicted center of the stretching band at ν_S = 2448 cm^{-1}[50] is still 50 cm^{-1} smaller than the experimental value of 2498 cm^{-1},[19] which indicates that the H-bond strength is still overestimated by SCAN functional. Here, the above overestimated H-bond strength is largely corrected by the SCAN0 functional. The SCAN0 functional yields a stretching band centered at ν_S = 2507 cm^{-1}, which is in quantitative agreement with the experimental measurement. We attribute the improvement of the IR stretching band to the reduced self-interaction error by mixing a fraction of exact exchange in SCAN0, which mitigates the overestimated directional H-bonding strength. The softened water structure reduces the tendency of a proton within a water molecule to be donated to the neighboring water molecules and therefore hinders the vibration of protons as described by the stretching mode. Consistently, the decompositions of the IR spectra show that the improved stretching band originates from both the inter- and intramolecular contributions, which show a comparable blue-shift compared to that from the SCAN functional. This is because the less polarized H-bond network by SCAN0 makes a proton less likely to be donated to a neighboring water molecule and therefore increases the covalent bond strength as evidenced by the shortened OH bond length as shown in Table 1 or Figure 2. Therefore, it is not surprising that the intra- and intermolecular contributions to the stretching mode both become stiffened by the exact exchange in SCAN0.

We next draw our attention to the bending band of the IR spectrum, which is centered ~1200 cm^{-1}. Compared with the prediction by SCAN, the SCAN0 functional predicts an improved bending band. In particular, a significant enhancement can be identified in the intensity of the bending motion, which should be attributed to the improved H-bond network as well. Unlike the stretching band, the intra- and intermolecular contributions to the bending mode are competing with each other. The intra- and intermolecular dipoles have positive and negative correlations, respectively, which results in the opposite signs of the above two decompositions at roughly the same frequencies, as shown in Figure 3b. In crystalline ice, the intensity of the bending band is rather weak due to the strong intermolecular dipole−dipole correlation while the contrary is true in liquid water.[97,98] Because of the artificially strengthened H-bond network described by the SCAN functional, the intermolecular negative dipolar correlation is overestimated, which results in a weaker spectral intensity than that of experiment as shown in Figure 3a. Whereas, the softened structure of liquid water predicted by SCAN0 suppresses the negative correlation of intermolecular dipole moments and instead promotes the positive intramolecular dipole correlation. The above effect gives an important correction to the bending band of the IR spectrum as seen by the increased overall intensity toward the experimental direction.

Finally, we analyze spectral features in the low-frequency range, which are composed of the hindered translation band centered at ~200 cm^{-1} and the libration band center at ~500 cm^{-1}. It can be seen that the IR spectrum predicted by SCAN0 also shows better agreement with experiment compared to SCAN. In particular, the improvement in the main peak of the libration band is more noticeable. The decompositions of the IR spectrum into its inter- and intramolecular contributions show that the improvement originates from the intramolecular part. The positive intramolecular dipolar correlation is slightly enhanced under the weakened H-bond network by SCAN0, which hampers the water libration motion by shifting its band to a slightly higher frequency range.

Besides the improvement to the IR spectrum compared to SCAN, our SCAN0 DPMD simulation also captures the spectral difference between heavy and light water accurately as shown in Figures 3a and 3c. Because of the lighter mass of H than D, all the four spectral features in light water are systematically higher than those in heavy water. A difference can be identified in the stretching/bending band between light water at 3475/1667 cm^{-1} and heavy water at 2507/1219 cm^{-1}, respectively, which originates from molecular vibration in the vapor phase. In the low frequencies range, the spectral differences are relatively smaller. The translation/libration band is located at 208/675 cm^{-1} for light water and 227/486 cm^{-1} for heavy water. Not surprisingly, the reduced isotope effects are due to the fact that collective vibrations become more important in the lower frequency region, which is less affected by the mass difference between H and D.

Diffusivity. The self-diffusion coefficient is an important physical quantity that differentiates liquid water from crystalline ice. It has been well recognized that the calculation of the diffusion coefficient of water is a challenge for AIMD. The difficulty lies in the fact that the predicted diffusivity of water, which is modeled by finite box size under periodic boundary conditions, must be corrected before a meaningful comparison can be made with the experimental value D_∞, which corresponds to the diffusivity of water in its thermodynamic limit. Based on the Kirkwood−Riseman theory of polymer diffusion, the correction term adopts the form of $D_\infty = D(L) + \frac{k_B T \zeta}{6\pi\eta L}$,[99] where $D(L)$ is the diffusivity obtained in a system with cell length L, ζ is a numerical coefficient of 2.837, and η is the shear viscosity. In the above, $D(L)$ approaches D_∞ rather slowly with a $1/L$ scaling. In practice, D_∞ is obtained by linear interpolation. Therefore, the accurate prediction demands water models of large box size containing thousands of molecules, which is computational challenging for DFT-based AIMD. In this work, utilizing the SCAN0 deep potential model, a series of simulations with cell sizes ranging from 64 to 4096 water molecules were conducted for both light and heavy water. For each cell size, four independent simulations were conducted for 300 ps. The diffusion coefficients were calculated by linear fittings of the mean-square displacement of the molecular center of mass in the time interval of 1−10 ps. The error bars were estimated as the root-mean-square error of the four diffusion coefficients obtained from the four independent trajectories. As shown in Figure 4, the extrapolated values of D to infinite system size are 0.26 and 0.29 $Å^2$/ps for D_2O and H_2O, respectively, which is in qualitative agreement with the 300 K experimental result of 0.20 and 0.24 $Å^2$/ps for D_2O and H_2O.[85] It can be noticed that the diffusion coefficient 0.29 $Å^2$/ps of light water predicted by the SCAN0 DPMD simulation at 330 K is slightly larger than the 0.26 $Å^2$/ps predicted by the SCAN neural network[87] at 330 K. This is because the more weakly H-bonded water molecules

https://doi.org/10.1021/acs.jpcb.1c03884
J. Phys. Chem. B XXXX, XXX, XXX−XXX

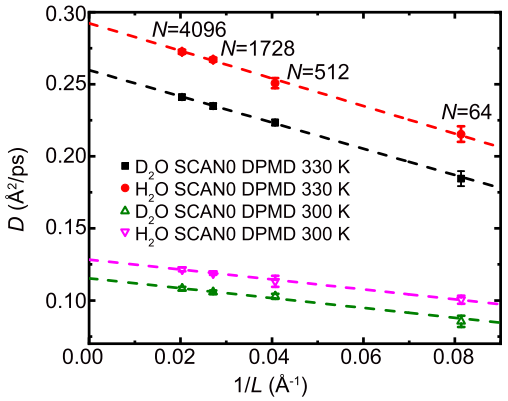

Figure 4. Diffusion coefficients of liquid H_2O and D_2O from SCAN0 DPMD simulation at 330 and 300 K with different sizes of the simulation cell.

described by the SCAN0 than that by the SCAN functional promotes the diffusion of water.

The diffusion coefficient displays the translational dynamics of the H-bonds, while the rotational correlation time reflects the rotational dynamics which can be calculated by the integration of the second-order orientational correlation function as

$$\tau_2 = \int_0^\infty \langle P_2[\mathbf{u}(0)\cdot\mathbf{u}(t)]\rangle \, dt$$

where P_2 is the second Legendre polynomial and $\mathbf{u}$ is the unit vector along the molecular vector of interest. In this work, $\mathbf{u}$ is chosen to be the unit vector along the OH covalent bonds of the water molecules. The values of τ_2 for heavy and light water obtained from the SCAN0 DPMD simulation are 1.9 and 1.7 ps, respectively, which is in qualitative agreement with the nuclear magnetic resonance experimental values of 2.4 ps[86] for heavy water and 1.7−2.6 ps[80,81] for light water. Compared to the τ_2 of 3.3 ps for light water predicted by the SCAN neural network[87] at 330 K, the τ_2 of 1.7 ps predicted by our SCAN0 DPMD simulation indicates a faster rotational dynamics, which is in accordance with the faster translations dynamics by SCAN0 and can also be explained by the weaker hydrogen bonds due to the mitigation of self-interaction error.

Electronic Properties Predicted at 330 K. *Electronic DOS and Bandgaps.* The electronic structure of liquid water can be efficiently probed by spectroscopy experiments that involving single-particle excitations. The valence band and conduction band can be extracted from the experimental data obtained by direct and indirect PES measurements,[89] respectively. Moreover, the energy difference between the conduction band minimum and valence band maximum gives the quasiparticle (QP) bandgap. Physically, PES measures the energy of adding or removing a single-particle excitation from the system, which can be understood as electron or hole quasiparticles dressed by interactions with the system. In practice, these quasiparticles can be described by Hedin's GW approximation[66] within many-body perturbation theory. Within the GW approximation, the QP energies are typically calculated as one-shot correction without self-consistency (i.e., G_0W_0) on top of a DFT mean field, making electronic structure calculations within GW an important benchmark for the accuracy of the DFT electronic ground state.

In Figure 5, we present the DOS predicted by both DFT and G_0W_0 calculations, with the molecular configurations obtained from SCAN AIMD,[14] SCAN0 DPMD, and SCAN0 PI-DPMD simulations. The experimental PES result[88] is also presented for comparison. In Figure 5, the four peaks with energies smaller than zero belong to the valence band and can be assigned to the $2a_1$, $1b_2$, $3a_1$, and $1b_1$ orbitals based on the spatial symmetries of a water molecule, while the peaks having energies above the Fermi level belong to the conduction bands. The DFT results in Figure 5 show that as the functional changes from SCAN to SCAN0, the energy of the $2a_1$ orbital with respect to the $1b_1$ orbital changes from −18.9 to −19.4 eV, the latter of which is closer to the experimental result of −19.7 eV. Therefore, SCAN0 provides a more precise description of the strongly bound $2a_1$ peak than SCAN. The above can be explained by the fact that the $2a_1$ orbital is primarily composed of the 2s electrons of the oxygen atom, which are corrected significantly when the self-interaction error is mitigated by the exact exchange in SCAN0. The decrease of

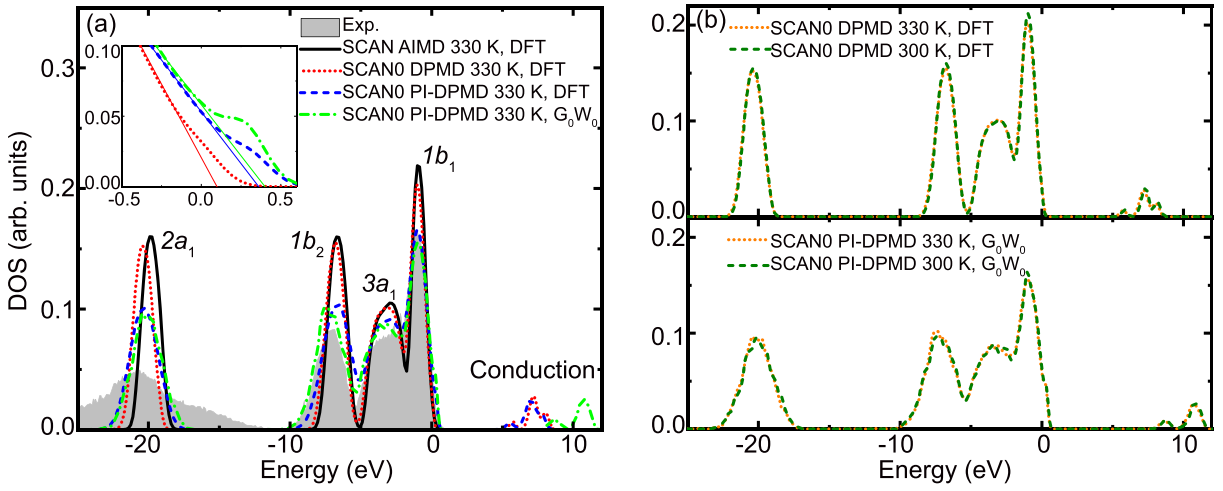

Figure 5. (a) Electronic DOS of liquid water calculated by using the DFT and G_0W_0 methods based on the configurations predicted by SCAN AIMD,[14] SCAN0 DPMD, and SCAN0 PI-DPMD at 330 K as well as the experimental photoemission spectra.[88] The $1b_1$ peak position is used to align all calculations. The inset shows the linearly extrapolated threshold of the valence band maximum. (b) Comparisons between the electronic DOS calculated by using the configurations predicted at 330 and 300 K.

https://doi.org/10.1021/acs.jpcb.1c03884
J. Phys. Chem. B XXXX, XXX, XXX−XXX

the $2a_1$ energy explains the increased covalency by SCAN0, as the bonding pairs of electrons in a water molecule are primarily come from a combination of the $1b_2$ and $2a_1$ orbitals with a small proportion of the $3a_1$ orbital.[93] When NQEs are incorporated by the PI method, the distribution of the DOS is broadened and closer to the experimental result because NQEs enable the protons to explore more configuration space that is inaccessible in classical simulations. The broadening of the $2a_1$ and $1b_2$ orbitals are more obvious than the broadening of the $3a_1$ and $1b_1$ orbitals because the $2a_1$ and $1b_2$ orbitals are highly correlated to the bonding pairs of electrons and the hydrogen atoms in water molecules are delocalized significantly under NQEs. It needs to be noted that even with the broadening by NQEs, the calculated $2a_1$ peak is still narrower than the experimental result as shown in Figure 5a. This is because the energy loss of the initial $1b_1$ electrons results in a broad background of the experimental $2a_1$ feature,[12] which is not accounted for in our calculations.

For the SCAN0 PI-DPMD configurations, when the calculation method of the electronic structure changes from DFT to G_0W_0, the DOS associated with the valence states barely changes (the small differences between theses two results are within the margin of error associated with the statistical fluctuations, as G_0W_0 results are only averaged on eight snapshots), but the bandgap at the G_0W_0 level is significantly improves compared to DFT. While Kohn−Sham DFT is a formally exact theory for the ground-state total energy and density of a material, a Kohn−Sham electronic structure calculation at fixed electron number fails to capture the contribution to the fundamental bandgap from the discontinuity of the exact exchange-correlation potential under a change of electron number.[100,101] As a result, it is well-known that the bandgaps in insulating systems are underestimated.[102,103] The underestimations are noticeable in DFT calculations by LDA and GGA functionals and become less severe when the nonlocal XC effects are considered in generalized Kohn−Sham such as hybrid functionals with exact exchange.[104] The above is well illustrated by the comparison of the bandgap of 4.9 eV predicted by the meta-GGA SCAN functional[14] with the bandgap of 5.7 eV predicted by the hybrid SCAN0 functional, the latter of which is closer to the experimental result of 8.7 ± 0.5 eV.[89] It needs to be mentioned that the above bandgaps of 4.9[14] and 5.7 eV are obtained by simply taking the energy difference between the highest occupied orbital and lowest unoccupied orbital. In practice, a better way to calculate the bandgap is determining the position of the valence band maximum and conduction band minimum as the linearly extrapolated threshold as shown in the inset of Figure 5, which leads to faster convergence of the valence band maximum and conduction band minimum values with respect to cell sizes.[12,105] In this way, the bandgaps predicted by DFT based on the SCAN0 DPMD and PI-DPMD configurations are 5.1 and 4.6 eV, respectively. The quantum simulation reduces the bandgap, in agreement with previous findings.[12] The G_0W_0 calculation corrects the bandgap from 4.6 to 7.5 eV, which is close to the experimental result of 8.7 ± 0.5 eV.[89] Further improvement in the bandgap can be achieved by the quasiparticle self-consistent GW method with vertex corrections.[12] However, that is beyond the scope of this work.

Dielectric Constant. The large dielectric constant is another anomalous property of liquid water, whose value is significantly larger than other materials with comparable electric dipoles.[83] A microscopic insight into the dielectric constant of liquid water is essential for understanding its properties as a solvent. However, the *ab initio* calculation of the dielectric constant, ϵ, of liquid water has long been a challenging prediction. Under the periodic boundary condition, the dielectric constant is connected with the fluctuations of electric dipole moments of water molecules and their correlations. On the basis of linear response theory, the dielectric constant of water can be calculated by the equation[106−108]

$$\epsilon = \epsilon_\infty + \frac{4\pi}{3}\frac{\rho\langle\mu^2\rangle G_k}{k_B T} \tag{2}$$

where $\epsilon_\infty = 1.77$, μ is the molecular dipole moment, ρ is the molecular number density, k_B is the Boltzmann's constant, and T is the temperature. G_k is the large-r limit of the correlation factor $G_k(r)$, which contains the integration of correlations among the dipole moments of different molecules and can be calculated as[106]

$$G_k(r) = 1 + \frac{\int d\mathbf{r}\langle\sum_{i\neq j}\boldsymbol{\mu}_i\cdot\boldsymbol{\mu}_j\delta(\mathbf{r}+\mathbf{r}_i-\mathbf{r}_j)\rangle}{N\langle\mu^2\rangle}$$

$G_k(r) = 1$ indicates there is no correlation between the dipoles of different molecules. In liquid water, the dipoles are highly correlated due to the H-bond network. The resulting $G_k(r)$ is significantly larger than 1, which gives rise to the large dielectric constant. In the above, the dipole moment can be rigorously derived from ion positions and Wannier centers that representing electron positions. Previous studies have shown that ϵ can be qualitatively computed by a 64-molecule cell,[106] but large error bars remain due to a relatively small cell and a short trajectory. The difficulty lies in the fact that the correlation function converges rather slowly with r for correlated dipoles as shown in Figure 6. Utilizing the

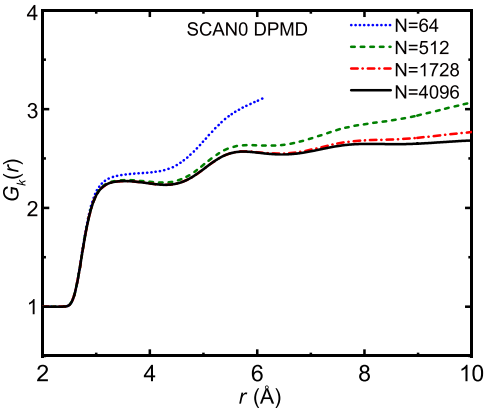

Figure 6. $G_k(r)$ of liquid water predicted by SCAN DPMD simulations with different cell sizes.

SCAN0 DPMD and PI-DPMD simulation, we calculated the dielectric constants of water with simulation cells containing 64−4096 molecules at 330 K. Each SCAN0 classical simulation lasted for 2 ns, and each SCAN0 quantum simulation lasted for 500 ps. It can be seen that ϵ converges slowly at the correlation distance r = 10 Å when the 4096-molecule cell is adopted. The SCAN0 classical and quantum simulation yield a dielectric constant of 76.83 and 84.34, respectively, which is close to the experimental result of 78.39.[83] As shown by the factor $\langle\mu^2\rangle G_k(r)$ in eq 2, the large dielectric constant of liquid water is contributed by both the

https://doi.org/10.1021/acs.jpcb.1c03884
J. Phys. Chem. B XXXX, XXX, XXX−XXX

molecular dipole moment and $G_k(r)$. The values of $G_k(r)$ predicted by SCAN0 classical and quantum simulations are 2.68 and 2.67, respectively, while the values of $\langle \mu^2 \rangle$ obtained from SCAN0 classical and quantum simulations are 8.83 and 9.66 D^2, respectively.

Properties Predicted at 300 K. The structure of liquid water predicted by the SCAN0 functional at 300 K is more overstructured compared to that at 330 K as shown by the RDFs in Figure 2. This is because the weaker thermal fluctuations at a lower temperature break fewer hydrogen bonds, which results in a more tetrahedral-like liquid structure. The differences between the RDFs predicted by the SCAN0 functional at 300 K with the experimental results at 298 K indicate that the hydrogen bond strength is still overestimated by the SCAN0 functional. The stronger hydrogen bonds at 300 K slow down the diffusion of the water molecules as illustrated by the smaller diffusion coefficient and larger rotational correlation time in Table 1. Compared to the IR spectra predicted at 330 K, the 300 K results agree better with the 298 K experimental spectra as displayed in Figure 3. Specifically, the vibrational frequency of the O−H/O−D stretching mode decreases due to the strengthening of the hydrogen bond; the intensity of the IR spectra increases because the intensity is calculated by using dipolar correlation dividing the temperature as shown by eq 1. The dielectric constant increases when the temperature decreases as shown in Table 1, which is caused by the increased molecular dipole moment, the stronger correlations between the dipoles of different molecules, and the decreased temperature (see eq 2).

The differences between the 330 K classical results and the 300 K quantum results predicted by the SCAN0 functional suggest that increasing the simulation temperature by 30 K does not have the equivalent effect of including nuclear quantum effects, which agrees with the findings in refs 87 and 109. The overstructured H-bond network of liquid water predicted by the SCAN0 functional at 300 K reveals clearly the deficiency of the SCAN0 functional. Compared to DFT functionals at the lower rung of Jacob's ladder of the GGA or meta-GGA level, the improvement of predicted water properties by the SCAN0 functional are qualitatively similar to those by revPBE0 functional with a D3 dispersion correction[92] and the PBE0 functional with a TS vdW correction.[61] However, the construction of SCAN0 functional is motivated by satisfying as many physical constraints as possible in one single functional and simultaneously avoiding many empirical parameters, which increases its transferability within the framework of DFT.

CONCLUSION

In conclusion, we have investigated liquid water based on DFT, in which the hybrid meta-GGA functional, SCAN0, was employed to approximate the exchange-correlation effect among electrons. The molecular structure of the liquid, the dynamics of the H-bond network, and the electronic properties of water were predicted and compared to available experimental measurements. In particular, we applied deep neural networks as implemented in the DeePMD and Deep Wannier methods, which were trained on the potential energy surface and electronic structure obtained for the electronic ground state described by SCAN0-DFT. The applications of the deep neural network potentials enable us to model water in much larger simulation boxes with significantly longer simulation time than those in regular DFT, which thereby enabled prediction of the macroscopic water properties by approaching the thermodynamic limit.

In addition to the existing 17 constraints satisfied by the SCAN functional, the nonlocal exact exchange mixed in SCAN0 further alleviates the self-interaction error. The reduced molecular polarizability by using SCAN0 softens the H-bond network of water toward the experimental direction as evidenced by the comparison of predicted RDFs with those obtained in scattering experiments. Because SCAN0 water is more loosely bound by the H-bond network, the water molecules are more diffusive and less correlated in spatial and temporal dimensions. The improvements in water dynamics have been demonstrated in IR spectra and diffusivity by comparison between theory and experiments. The spatial correlations, as represented by the dipole−dipole correlation in the dielectric response, were also accurately determined. Moreover, the predicted static dielectric constant is in good agreement with experiments. The electronic band structure and bandgap of water were determined by the GW self-energy approach as implemented in the Berkeley GW code package, which agree well with the PES experimental measurements. In all predicted static properties, the effects of including NQEs were found to give rise to mainly a broadening effect due to the delocalized protons as widely reported in the literature.

Our studies present the state-of-the-art theoretical modeling of water on the fourth rung of Jacob's ladder. Although there is improved accuracy in predicted water properties, some important discrepancies remain. The differences between the simulation results at 300 K with the 298/300 K experimental results indicate that the predicted H-bond network by SCAN0 is still slightly overstructured. The water density predicted by SCAN0 is improved over that by SCAN, but it is still a little overestimated. To address these remaining issues, more sophisticated treatment of the self-interaction correction and long-range van der Waals interactions should be included in DFT along with nonlocal exchange-correlation functional constructions at higher rungs of Jacob's ladder.

AUTHOR INFORMATION

Corresponding Authors

Michael L. Klein − *Department of Physics and Institute for Computational Molecular Science, Temple University, Philadelphia, Pennsylvania 19122, United States;* orcid.org/0000-0002-0027-9262; Email: mlklein@temple.edu

Xifan Wu − *Department of Physics, Temple University, Philadelphia, Pennsylvania 19122, United States;* orcid.org/0000-0001-6561-8942; Email: xifan.wu@temple.edu

Authors

Chunyi Zhang − *Department of Physics, Temple University, Philadelphia, Pennsylvania 19122, United States;* orcid.org/0000-0003-4146-703X

Fujie Tang − *Department of Physics, Temple University, Philadelphia, Pennsylvania 19122, United States;* orcid.org/0000-0001-9761-5359

Mohan Chen − *HEDPS, Center for Applied Physics and Technology, College of Engineering, Peking University, Beijing 100871, China*

Jianhang Xu − *Department of Physics, Temple University, Philadelphia, Pennsylvania 19122, United States*

https://doi.org/10.1021/acs.jpcb.1c03884
J. Phys. Chem. B XXXX, XXX, XXX−XXX

Linfeng Zhang − *Program in Applied and Computational Mathematics, Princeton University, Princeton, New Jersey 08544, United States;* orcid.org/0000-0002-8470-5846
Diana Y. Qiu − *Department of Mechanical Engineering and Materials Science, Yale University, New Haven, Connecticut 06520, United States*
John P. Perdew − *Department of Physics and Department of Chemistry, Temple University, Philadelphia, Pennsylvania 19122, United States*

Complete contact information is available at: https://pubs.acs.org/10.1021/acs.jpcb.1c03884

Notes

The authors declare no competing financial interest.

■ ACKNOWLEDGMENTS

This work was supported by National Science Foundation through Awards DMR-2053195 and DMR-1552287. This research used resources of the National Energy Research Scientific Computing Center (NERSC), which is supported by the U.S. Department of Energy (DOE), Office of Science, under Contract DE-AC02-05CH11231. The work of F.T. and M.L.K. was supported by the Computational Chemical Center: Chemistry in Solution and at Interfaces funded by the DOE under Award DESC0019394. The work of J.P.P. was supported by the U.S. National Science Foundation under Grant DMR-1939528, with a contribution from CTMC - Division of Chemistry. The work of D.Y.Q. was supported by the Center for Computational Study of Excited State Phenomena in Energy Materials (CSEPEM), which is funded by the U.S. Department of Energy, Office of Science, Basic Energy Sciences, Materials Sciences and Engineering Division, under Contract DE-AC02-05CH11231. This research includes calculations performed on HPC resources supported in part by the National Science Foundation through major research instrumentation grant 1625061 and by the U.S. Army Research Laboratory under Contract W911NF-16-2-0189. This research used resources of the Oak Ridge Leadership Computing Facility at the Oak Ridge National Laboratory, which is supported by the Office of Science of the U.S. Department of Energy under Contract DE-AC05-00OR22725. We thank Annabella Selloni, Marcos F. Calegari Andrade, Athanassios Z. Panagiotopoulos, Roberto Car, and members of the Princeton "Chemistry in Solution and at Interfaces" (CSI) Center for fruitful discussions.

■ REFERENCES

(1) Franks, F. *Water: A Matrix of Life*; Royal Society of Chemistry: 2007.
(2) Lynden-Bell, R. M.; Morris, S. C.; Barrow, J. D.; Finney, J. L.; Harper, C. *Water and Life: the Unique Properties of H_2O*; CRC Press: 2010.
(3) Geissler, P. L. Autoionization in Liquid Water. *Science* **2001**, *291*, 2121−2124.
(4) Chen, M.; Zheng, L.; Santra, B.; Ko, H.-Y.; DiStasio, R. A., Jr.; Klein, M. L.; Car, R.; Wu, X. Hydroxide Diffuses Slower than Hydronium in Water Because Its Solvated Structure Inhibits Correlated Proton Transfer. *Nat. Chem.* **2018**, *10*, 413−419.
(5) Camilloni, C.; Bonetti, D.; Morrone, A.; Giri, R.; Dobson, C. M.; Brunori, M.; Gianni, S.; Vendruscolo, M. Towards a Structural Biology of the Hydrophobic Effect in Protein Folding. *Sci. Rep.* **2016**, *6*, 28285.
(6) Baldwin, R. L.; Rose, G. D. How the Hydrophobic Factor Drives Protein Folding. *Proc. Natl. Acad. Sci. U. S. A.* **2016**, *113*, 12462−12466.
(7) Wernet, P.; Nordlund, D.; Bergmann, U.; Cavalleri, M.; Odelius, M.; Ogasawara, H.; Näslund, L. .; Hirsch, T. K.; Ojamäe, L.; Glatzel, P.; et al. The Structure of the First Coordination Shell in Liquid Water. *Science* **2004**, *304*, 995−999.
(8) Winter, B.; Weber, R.; Widdra, W.; Dittmar, M.; Faubel, M.; Hertel, I. Full Valence Band Photoemission from Liquid Water Using EUV Synchrotron Radiation. *J. Phys. Chem. A* **2004**, *108*, 2625−2632.
(9) Soper, A.; Benmore, C. Quantum Differences between Heavy and Light Water. *Phys. Rev. Lett.* **2008**, *101*, 065502.
(10) Skinner, L. B.; Huang, C.; Schlesinger, D.; Pettersson, L. G.; Nilsson, A.; Benmore, C. J. Benchmark Oxygen-Oxygen Pair-Distribution Function of Ambient Water from X-ray Diffraction Measurements with a Wide Q-Range. *J. Chem. Phys.* **2013**, *138*, 074506.
(11) DiStasio, R. A., Jr.; Santra, B.; Li, Z.; Wu, X.; Car, R. The Individual and Collective Effects of Exact Exchange and Dispersion Interactions on the Ab Initio Structure of Liquid Water. *J. Chem. Phys.* **2014**, *141*, 084502.
(12) Chen, W.; Ambrosio, F.; Miceli, G.; Pasquarello, A. Ab Initio Electronic Structure of Liquid Water. *Phys. Rev. Lett.* **2016**, *117*, 186401.
(13) Gillan, M. J.; Alfè, D.; Michaelides, A. Perspective: How Good is DFT for Water? *J. Chem. Phys.* **2016**, *144*, 130901.
(14) Chen, M.; Ko, H.-Y.; Remsing, R. C.; Calegari Andrade, M. F.; Santra, B.; Sun, Z.; Selloni, A.; Car, R.; Klein, M. L.; Perdew, J. P.; et al. Ab Initio Theory and Modeling of Water. *Proc. Natl. Acad. Sci. U. S. A.* **2017**, *114*, 10846−10851.
(15) Gaiduk, A. P.; Gustafson, J. A.; Gygi, F.; Galli, G. First-Principles Simulations of Liquid Water Using a Dielectric-Dependent Hybrid Functional. *J. Phys. Chem. Lett.* **2018**, *9*, 3068−3073.
(16) Luzar, A.; Chandler, D. Hydrogen-Bond Kinetics in Liquid Water. *Nature* **1996**, *379*, 55−57.
(17) Pettersson, L. G. M.; Henchman, R. H.; Nilsson, A. Water − The Most Anomalous Liquid. *Chem. Rev.* **2016**, *116*, 7459−7462.
(18) Nilsson, A.; Pettersson, L. G. M. The Structural Origin of Anomalous Properties of Liquid Water. *Nat. Commun.* **2015**, *6*, 8998.
(19) Max, J.-J.; Chapados, C. Isotope Effects in Liquid Water by Infrared Spectroscopy. III. H_2O and D_2O Spectra from 6000 to 0 cm^{-1}. *J. Chem. Phys.* **2009**, *131*, 184505.
(20) Bertie, J. E.; Lan, Z. Infrared Intensities of Liquids XX: The Intensity of the OH Stretching Band of Liquid Water Revisited, and the Best Current Values of the Optical Constants of H_2O(l) at 25 °C between 15,000 and 1 cm^{-1}. *Appl. Spectrosc.* **1996**, *50*, 1047−1057.
(21) Shen, Y. R.; Ostroverkhov, V. Sum-Frequency Vibrational Spectroscopy on Water Interfaces: Polar Orientation of Water Molecules at Interfaces. *Chem. Rev.* **2006**, *106*, 1140−1154.
(22) Tang, F.; Ohto, T.; Sun, S.; Rouxel, J. R.; Imoto, S.; Backus, E. H. G.; Mukamel, S.; Bonn, M.; Nagata, Y. Molecular Structure and Modeling of Water-Air and Ice-Air Interfaces Monitored by Sum-Frequency Generation. *Chem. Rev.* **2020**, *120*, 3633−3667.
(23) Yang, S.; Chen, M.; Su, Y.; Xu, J.; Wu, X.; Tian, C. Stabilization of Hydroxide Ions at the Interface of a Hydrophobic Monolayer on Water via Reduced Proton Transfer. *Phys. Rev. Lett.* **2020**, *125*, 156803.
(24) Woutersen, S. Femtosecond Mid-IR Pump-Probe Spectroscopy of Liquid Water: Evidence for a Two-Component Structure. *Science* **1997**, *278*, 658−660.
(25) Car, R.; Parrinello, M. Unified Approach for Molecular Dynamics and Density-Functional Theory. *Phys. Rev. Lett.* **1985**, *55*, 2471−2474.
(26) Hohenberg, P.; Kohn, W. Inhomogeneous Electron Gas. *Phys. Rev.* **1964**, *136*, B864.
(27) Kohn, W.; Sham, L. J. Self-Consistent Equations Including Exchange and Correlation Effects. *Phys. Rev.* **1965**, *140*, A1133.

(28) Perdew, J. P.; Schmidt, K. Jacob's Ladder of Density Functional Approximations for the Exchange-Correlation Energy. *AIP Conf. Proc.* **2000**, *577*, 1−20.
(29) Ceperley, D. M.; Alder, B. Ground State of the Electron Gas by a Stochastic Method. *Phys. Rev. Lett.* **1980**, *45*, 566.
(30) Perdew, J. P.; Zunger, A. Self-Interaction Correction to Density-Functional Approximations for Many-Electron Systems. *Phys. Rev. B: Condens. Matter Mater. Phys.* **1981**, *23*, 5048.
(31) Laasonen, K.; Csajka, F.; Parrinello, M. Water Dimer Properties in the Gradient-Corrected Density Functional Theory. *Chem. Phys. Lett.* **1992**, *194*, 172−174.
(32) Laasonen, K.; Parrinello, M.; Car, R.; Lee, C.; Vanderbilt, D. Structures of Small Water Clusters Using Gradient-Corrected Density Functional Theory. *Chem. Phys. Lett.* **1993**, *207*, 208−213.
(33) Becke, A. D. Density-Functional Exchange-Energy Approximation with Correct Asymptotic Behavior. *Phys. Rev. A: At., Mol., Opt. Phys.* **1988**, *38*, 3098.
(34) Lee, C.; Yang, W.; Parr, R. G. Development of the Colle-Salvetti Correlation-Energy Formula into a Functional of the Electron Density. *Phys. Rev. B: Condens. Matter Mater. Phys.* **1988**, *37*, 785.
(35) Perdew, J. P.; Burke, K.; Ernzerhof, M. Generalized Gradient Approximation Made Simple. *Phys. Rev. Lett.* **1996**, *77*, 3865−3868.
(36) Zhang, Y.; Yang, W. Comment on "Generalized Gradient Approximation Made Simple. *Phys. Rev. Lett.* **1998**, *80*, 890−890.
(37) Wang, J.; Román-Pérez, G.; Soler, J. M.; Artacho, E.; Fernández-Serra, M.-V. Density, Structure, and Dynamics of Water: The Effect of van der Waals Interactions. *J. Chem. Phys.* **2011**, *134*, 024516.
(38) Grimme, S. Accurate Description of van der Waals Complexes by Density Functional Theory Including Empirical Corrections. *J. Comput. Chem.* **2004**, *25*, 1463−1473.
(39) Grimme, S.; Antony, J.; Ehrlich, S.; Krieg, H. A Consistent and Accurate *Ab Initio* Parametrization of Density Functional Dispersion Correction (DFT-D) for the 94 Elements H-Pu. *J. Chem. Phys.* **2010**, *132*, 154104.
(40) Tkatchenko, A.; Scheffler, M. Accurate Molecular Van Der Waals Interactions from Ground-State Electron Density and Free-Atom Reference Data. *Phys. Rev. Lett.* **2009**, *102*, 073005.
(41) Galib, M.; Duignan, T. T.; Misteli, Y.; Baer, M. D.; Schenter, G. K.; Hutter, J.; Mundy, C. J. Mass Density Fluctuations in Quantum and Classical Descriptions of Liquid Water. *J. Chem. Phys.* **2017**, *146*, 244501.
(42) Sun, J.; Ruzsinszky, A.; Perdew, J. P. Strongly Constrained and Appropriately Normed Semilocal Density Functional. *Phys. Rev. Lett.* **2015**, *115*, 036402.
(43) Sun, J.; Remsing, R. C.; Zhang, Y.; Sun, Z.; Ruzsinszky, A.; Peng, H.; Yang, Z.; Paul, A.; Waghmare, U.; Wu, X.; et al. Accurate First-Principles Structures and Energies of Diversely Bonded Systems from an Efficient Density Functional. *Nat. Chem.* **2016**, *8*, 831−836.
(44) Zheng, L.; Chen, M.; Sun, Z.; Ko, H.-Y.; Santra, B.; Dhuvad, P.; Wu, X. Structural, Electronic, and Dynamical Properties of Liquid Water by Ab Initio Molecular Dynamics Based on SCAN Functional within the Canonical Ensemble. *J. Chem. Phys.* **2018**, *148*, 164505.
(45) Xu, J.; Sun, Z.; Zhang, C.; DelloStritto, M.; Lu, D.; Klein, M. L.; Wu, X. Importance of Nuclear Quantum Effects on the Hydration of Chloride Ion. *Phys. Rev. Mater.* **2021**, *5*, L012801.
(46) Piaggi, P. M.; Panagiotopoulos, A. Z.; Debenedetti, P. G.; Car, R. Phase Equilibrium of Water with Hexagonal and Cubic Ice Using the SCAN Functional. *J. Chem. Theory Comput.* **2021**, *17*, 3065−3077.
(47) Perdew, J. P.; Zunger, A. Self-Interaction Correction to Density-Functional Approximations for Many-Electron Systems. *Phys. Rev. B: Condens. Matter Mater. Phys.* **1981**, *23*, 5048−5079.
(48) Sharkas, K.; Wagle, K.; Santra, B.; Akter, S.; Zope, R. R.; Baruah, T.; Jackson, K. A.; Perdew, J. P.; Peralta, J. E. Self-Interaction Error Overbinds Water Clusters but Cancels in Structural Energy Differences. *Proc. Natl. Acad. Sci. U. S. A.* **2020**, *117*, 11283−11288.
(49) Zhang, C.; Donadio, D.; Gygi, F.; Galli, G. First Principles Simulations of the Infrared Spectrum of Liquid Water Using Hybrid Density Functionals. *J. Chem. Theory Comput.* **2011**, *7*, 1443−1449.
(50) Xu, J.; Chen, M.; Zhang, C.; Wu, X. First-Principles Study of the Infrared Spectrum in Liquid Water from a Systematically Improved Description of H-Bond Network. *Phys. Rev. B: Condens. Matter Mater. Phys.* **2019**, *99*, 205123.
(51) Lambros, E.; Hu, J.; Paesani, F. Assessing the Accuracy of the SCAN Functional for Water through a Many-body Analysis of the Adiabatic Connection Formula. *J. Chem. Theory Comput.* **2021**, *17*, 3739−3749.
(52) Li, X.-Z.; Walker, B.; Michaelides, A. Quantum Nature of the Hydrogen Bond. *Proc. Natl. Acad. Sci. U. S. A.* **2011**, *108*, 6369−6373.
(53) Ceriotti, M.; Cuny, J.; Parrinello, M.; Manolopoulos, D. E. Nuclear Quantum Effects and Hydrogen Bond Fluctuations in Water. *Proc. Natl. Acad. Sci. U. S. A.* **2013**, *110*, 15591−15596.
(54) Ceriotti, M.; Fang, W.; Kusalik, P. G.; McKenzie, R. H.; Michaelides, A.; Morales, M. A.; Markland, T. E. Nuclear Quantum Effects in Water and Aqueous Systems: Experiment, Theory, and Current Challenges. *Chem. Rev.* **2016**, *116*, 7529−7550.
(55) Marx, D.; Parrinello, M. Ab Initio Path Integral Molecular Dynamics: Basic Ideas. *J. Chem. Phys.* **1996**, *104*, 4077−4082.
(56) Ceriotti, M.; More, J.; Manolopoulos, D. E. I-PI A Python Interface for Ab Initio Path Integral Molecular Dynamics Simulations. *Comput. Phys. Commun.* **2014**, *185*, 1019−1026.
(57) Fecko, C. J.; Eaves, J. D.; Loparo, J. J.; Tokmakoff, A.; Geissler, P. L. Ultrafast Hydrogen-Bond Dynamics in the Infrared Spectroscopy of Water. *Science* **2003**, *301*, 1698−1702.
(58) Zhang, L.; Han, J.; Wang, H.; Car, R.; E, W. Deep Potential Molecular Dynamics: A Scalable Model with the Accuracy of Quantum Mechanics. *Phys. Rev. Lett.* **2018**, *120*, 143001.
(59) Zhang, L.; Lin, D.-Y.; Wang, H.; Car, R.; E, W. Active Learning of Uniformly Accurate Interatomic Potentials for Materials Simulation. *Phys. Rev. Materials* **2019**, *3*, 023804.
(60) Zhang, L.; Han, J.; Wang, H.; Saidi, W.; Car, R.; E, W. In *Advances in Neural Information Processing Systems 31*; Bengio, S., Wallach, H., Larochelle, H., Grauman, K., Cesa-Bianchi, N., Garnett, R., Eds.; Curran Associates, Inc.: 2018; pp 4436−4446.
(61) Ko, H.-Y.; Zhang, L.; Santra, B.; Wang, H.; E, W.; DiStasio, R. A., Jr.; Car, R. Isotope Effects in Liquid Water via Deep Potential Molecular Dynamics. *Mol. Phys.* **2019**, *117*, 3269−3281.
(62) Zhang, L.; Chen, M.; Wu, X.; Wang, H.; E, W.; Car, R. Deep Neural Network for the Dielectric Response of Insulators. *Phys. Rev. B: Condens. Matter Mater. Phys.* **2020**, *102*, 041121.
(63) Marzari, N.; Vanderbilt, D. Maximally Localized Generalized Wannier Functions for Composite Energy Bands. *Phys. Rev. B: Condens. Matter Mater. Phys.* **1997**, *56*, 12847−12865.
(64) Marzari, N.; Mostofi, A. A.; Yates, J. R.; Souza, I.; Vanderbilt, D. Maximally Localized Wannier Functions: Theory and Applications. *Rev. Mod. Phys.* **2012**, *84*, 1419−1475.
(65) Staroverov, V. N.; Scuseria, G. E.; Tao, J.; Perdew, J. P. Comparative Assessment of a New Nonempirical Density Functional: Molecules and Hydrogen-Bonded Complexes. *J. Chem. Phys.* **2003**, *119*, 12129−12137.
(66) Hedin, L. New Method for Calculating the One-Particle Green's Function with Application to the Electron-Gas Problem. *Phys. Rev.* **1965**, *139*, A796−A823.
(67) Hybertsen, M. S.; Louie, S. G. Electron Correlation in Semiconductors and Insulators: Band Gaps and Quasiparticle Energies. *Phys. Rev. B: Condens. Matter Mater. Phys.* **1986**, *34*, 5390−5413.
(68) Deslippe, J.; Samsonidze, G.; Strubbe, D. A.; Jain, M.; Cohen, M. L. BerkeleyGW: A Massively Parallel Computer Package for the Calculation of the Quasiparticle and Optical Properties of Materials and Nanostructures. *Comput. Phys. Commun.* **2012**, *183*, 1269−1289.
(69) Zhang, C.; Zhang, L.; Xu, J.; Tang, F.; Santra, B.; Wu, X. Isotope Effects in X-ray Absorption Spectra of Liquid Water. *Phys. Rev. B: Condens. Matter Mater. Phys.* **2020**, *102*, 115155.

https://doi.org/10.1021/acs.jpcb.1c03884
J. Phys. Chem. B XXXX, XXX, XXX−XXX

(70) Giannozzi, P.; Andreussi, O.; Brumme, T.; Bunau, O.; Nardelli, M. B.; Calandra, M.; Car, R.; Cavazzoni, C.; Ceresoli, D.; Cococcioni, M.; et al. Advanced Capabilities for Materials Modelling with Quantum ESPRESSO. *J. Phys.: Condens. Matter* **2017**, *29*, 465901.
(71) Hamann, D.; Schlüter, M.; Chiang, C. Norm-Conserving Pseudopotentials. *Phys. Rev. Lett.* **1979**, *43*, 1494.
(72) Vanderbilt, D. Optimally Smooth Norm-Conserving Pseudopotentials. *Phys. Rev. B: Condens. Matter Mater. Phys.* **1985**, *32*, 8412.
(73) Wang, H.; Zhang, L.; Han, J.; E, W. DeePMD-kit: A Deep Learning Package for Many-body Potential Energy Representation and Molecular Dynamics. *Comput. Phys. Commun.* **2018**, *228*, 178−184.
(74) Kingma, D. P.; Ba, J. Adam: A Method for Stochastic Optimization. *arXiv:1412.6980*, **2017**.
(75) Ceriotti, M.; Bussi, G.; Parrinello, M. Nuclear Quantum Effects in Solids Using a Colored-Noise Thermostat. *Phys. Rev. Lett.* **2009**, *103*, 030603.
(76) Ceriotti, M.; Manolopoulos, D. E. Efficient First-Principles Calculation of the Quantum Kinetic Energy and Momentum Distribution of Nuclei. *Phys. Rev. Lett.* **2012**, *109*, 100604.
(77) Ceriotti, M.; Bussi, G.; Parrinello, M. Langevin Equation with Colored Noise for Constant-Temperature Molecular Dynamics Simulations. *Phys. Rev. Lett.* **2009**, *102*, 020601.
(78) Ceriotti, M.; Bussi, G.; Parrinello, M. Colored-Noise Thermostats à la Carte. *J. Chem. Theory Comput.* **2010**, *6*, 1170−1180.
(79) Plimpton, S. Fast Parallel Algorithms for Short-Range Molecular Dynamics. *J. Comput. Phys.* **1995**, *117*, 1−19.
(80) Lankhorst, D.; Schriever, J.; Leyte, J. C. Determination of the Rotational Correlation Time of Water by Proton NMR Relaxation in $H_2{}^{17}O$ and Some Related Results. *Ber. Bunsen. Phys. Chem.* **1982**, *86*, 215−221.
(81) Smith, D.; Powles, J. Proton Spin-lattice Relaxation in Liquid Water and Liquid Ammonia. *Mol. Phys.* **1966**, *10*, 451−463.
(82) Badyal, Y.; Saboungi, M.-L.; Price, D.; Shastri, S.; Haeffner, D.; Soper, A. Electron Distribution in Water. *J. Chem. Phys.* **2000**, *112*, 9206−9208.
(83) Vidulich, G. A.; Evans, D. F.; Kay, R. L. The Dielectric Constant of Water and Heavy Water between 0 and 40°. *J. Phys. Chem.* **1967**, *71* (3), 656−662.
(84) Linstrom, P. J.; Mallard, W. G. The NIST Chemistry WebBook: A Chemical Data Resource on the Internet. *J. Chem. Eng. Data* **2001**, *46*, 1059−1063.
(85) Mills, R. Self-Diffusion in Normal and Heavy Water in the Range 1−45°. *J. Phys. Chem.* **1973**, *77*, 685−688.
(86) Ropp, J.; Lawrence, C.; Farrar, T. C.; Skinner, J. L. Rotational Motion in Liquid Water Is Anisotropic: A Nuclear Magnetic Resonance and Molecular Dynamics Simulation Study. *J. Am. Chem. Soc.* **2001**, *123*, 8047.
(87) Yao, Y.; Kanai, Y. Temperature Dependence of Nuclear Quantum Effects on Liquid Water via Artificial Neural Network Model Based on SCAN Meta-GGA Functional. *J. Chem. Phys.* **2020**, *153*, 044114.
(88) Winter, B.; Weber, R.; Widdra, W.; Dittmar, M.; Faubel, M.; Hertel, I. V. Full Valence Band Photoemission from Liquid Water Using EUV Synchrotron Radiation. *J. Phys. Chem. A* **2004**, *108*, 2625−2632.
(89) Bernas, A.; Ferradini, C.; Jay-Gerin, J.-P. On the Electronic Structure of Liquid Water: Facts and Reflections. *Chem. Phys.* **1997**, *222*, 151−160.
(90) Zeidler, A.; Salmon, P. S.; Fischer, H. E.; Neuefeind, J. C.; Simonson, J. M.; Markland, T. E. Isotope Effects in Water as Investigated by Neutron Diffraction and Path Integral Molecular Dynamics. *J. Phys.: Condens. Matter* **2012**, *24*, 284126.
(91) Wang, L.; Ceriotti, M.; Markland, T. E. Quantum Fluctuations and Isotope Effects in *Ab initio* Descriptions of Water. *J. Chem. Phys.* **2014**, *141*, 104502.
(92) Cheng, B.; Engel, E. A.; Behler, J.; Dellago, C.; Ceriotti, M. *Ab Initio* Thermodynamics of Liquid and Solid Water. *Proc. Natl. Acad. Sci. U. S. A.* **2019**, *116*, 1110−1115.
(93) Xu, J.; Zhang, C.; Zhang, L.; Chen, M.; Santra, B.; Wu, X. Isotope Effects in Molecular Structures and Electronic Properties of Liquid Water via Deep Potential Molecular Dynamics Based on the SCAN Functional. *Phys. Rev. B: Condens. Matter Mater. Phys.* **2020**, *102*, 214113.
(94) Markland, T. E.; Ceriotti, M. Nuclear Quantum Effects Enter the Mainstream. *Nat. Rev. Chem.* **2018**, *2*, 0109.
(95) Chen, W.; Sharma, M.; Resta, R.; Galli, G.; Car, R. Role of Dipolar Correlations in the Infrared Spectra of Water and Ice. *Phys. Rev. B: Condens. Matter Mater. Phys.* **2008**, *77*, 245114.
(96) Mcquarrie, D. A. *Statistical Mechanics*; University Science Books: Sausalito, CA, 2000.
(97) Mallamace, F.; Broccio, M.; Corsaro, C.; Faraone, A.; Majolino, D.; Venuti, V.; Liu, L.; Mou, C.-Y.; Chen, S.-H. Evidence of the Existence of the Low-density Liquid Phase in Supercooled, Confined Water. *Proc. Natl. Acad. Sci. U. S. A.* **2007**, *104*, 424−428.
(98) Imoto, S.; Xantheas, S. S.; Saito, S. Molecular Origin of the Difference in the HOH Bend of the IR Spectra between Liquid Water and Ice. *J. Chem. Phys.* **2013**, *138*, 054506.
(99) Yeh, I.-C.; Hummer, G. System-Size Dependence of Diffusion Coefficients and Viscosities from Molecular Dynamics Simulations with Periodic Boundary Conditions. *J. Phys. Chem. B* **2004**, *108*, 15873−15879.
(100) Perdew, J. P.; Parr, R. G.; Levy, M.; Balduz, J. L. Density-Functional Theory for Fractional Particle Number: Derivative Discontinuities of the Energy. *Phys. Rev. Lett.* **1982**, *49*, 1691−1694.
(101) Perdew, J. P.; Levy, M. Physical Content of the Exact Kohn-Sham Orbital Energies: Band Gaps and Derivative Discontinuities. *Phys. Rev. Lett.* **1983**, *51*, 1884−1887.
(102) Cohen, A. J.; Mori-Sanchez, P.; Yang, W. Insights into Current Limitations of Density Functional Theory. *Science* **2008**, *321*, 792−794.
(103) Swartz, C. W.; Wu, X. *Ab initio* Studies of Ionization Potentials of Hydrated Hydroxide and Hydronium. *Phys. Rev. Lett.* **2013**, *111*, 087801.
(104) Perdew, J. P.; Yang, W.; Burke, K.; Yang, Z.; Gross, E. K. U.; Scheffler, M.; Scuseria, G. E.; Henderson, T. M.; Zhang, I. Y.; Ruzsinszky, A.; et al. Understanding Band Gaps of Solids in Generalized Kohn-Sham Theory. *Proc. Natl. Acad. Sci. U. S. A.* **2017**, *114*, 2801−2806.
(105) Ambrosio, F.; Miceli, G.; Pasquarello, A. Redox Levels in Aqueous Solution: Effect of van der Waals Interactions and Hybrid Functionals. *J. Chem. Phys.* **2015**, *143*, 244508.
(106) Sharma, M.; Resta, R.; Car, R. Dipolar Correlations and the Dielectric Permittivity of Water. *Phys. Rev. Lett.* **2007**, *98*, 247401.
(107) Adams, D. J. Theory of the Dielectric Constant of Ice. *Nature* **1981**, *293*, 447.
(108) Neumann, M. Dipole Moment Fluctuation Formulas in Computer Simulations of Polar Systems. *Mol. Phys.* **1983**, *50*, 841−858.
(109) Ruiz Pestana, L.; Marsalek, O.; Markland, T. E.; Head-Gordon, T. The Quest for Accurate Liquid Water Properties from First Principles. *J. Phys. Chem. Lett.* **2018**, *9*, 5009−5016.

https://doi.org/10.1021/acs.jpcb.1c03884
J. Phys. Chem. B XXXX, XXX, XXX−XXX